Cancer Cell
Article

TAK1 Suppresses a NEMO-Dependent but NF-κB-Independent Pathway to Liver Cancer

Kira Bettermann,[1,13] Mihael Vucur,[1,13] Johannes Haybaeck,[4] Christiane Koppe,[1] Jörn Janssen,[1] Felix Heymann,[1] Achim Weber,[4] Ralf Weiskirchen,[2] Christian Liedtke,[1] Nikolaus Gassler,[3] Michael Müller,[5] Rita de Vos,[6] Monika Julia Wolf,[4] Yannick Boege,[4] Gitta Maria Seleznik,[4] Nicolas Zeller,[7] Daniel Erny,[7] Thomas Fuchs,[8] Stefan Zoller,[9] Stefano Cairo,[10] Marie-Annick Buendia,[10] Marco Prinz,[7] Shizuo Akira,[11] Frank Tacke,[1] Mathias Heikenwalder,[4,12] Christian Trautwein,[1] and Tom Luedde[1,*]

[1]Department of Internal Medicine III
[2]Institute of Clinical Chemistry and Pathobiochemistry
[3]Institute of Pathology
University Hospital RWTH Aachen, D-52074 Aachen, Germany
[4]Department of Pathology, Institutes of Neuropathology and Clinical Pathology, University Hospital Zurich, CH 8091 Zurich, Switzerland
[5]Department of Nutrition, Metabolism and Genomics, Wageningen University, 6709 PA Wageningen, the Netherlands
[6]Department of Pathology, University Hospitals, University of Leuven, B-3000 Leuven, Belgium
[7]Department of Neuropathology, University of Freiburg, D-79106 Freiburg, Germany
[8]Department of Computer Science, ETH Zurich, CH 8092 Zurich, Switzerland
[9]Transcriptomics, Bioinformatics Functional Genomics Center Zurich, CH 8057 Zurich, Switzerland
[10]Oncogenesis and Molecular Virology Unit, Institut Pasteur, and INSERM U579, F-75724 Paris, France
[11]Laboratory of Host Defense, WPI Immunology Frontier Research Center, Osaka University, J-565-0871 Osaka, Japan
[12]Present address: Institute of Virology, Helmholtz Center Munich, Technical University Munich, D-81675 Munich, Germany
[13]These authors contributed equally to this work
*Correspondence: tluedde@ukaachen.de
DOI 10.1016/j.ccr.2010.03.021

SUMMARY

The MAP3-kinase TGF-β-activated kinase 1 (TAK1) critically modulates innate and adaptive immune responses and connects cytokine stimulation with activation of inflammatory signaling pathways. Here, we report that conditional ablation of TAK1 in liver parenchymal cells (hepatocytes and cholangiocytes) causes hepatocyte dysplasia and early-onset hepatocarcinogenesis, coinciding with biliary ductopenia and cholestasis. TAK1-mediated cancer suppression is exerted through activating NF-κB in response to tumor necrosis factor (TNF) and through preventing Caspase-3-dependent hepatocyte and cholangiocyte apoptosis. Moreover, TAK1 suppresses a procarcinogenic and pronecrotic pathway, which depends on NF-κB-independent functions of the IκB-kinase (IKK)-subunit NF-κB essential modulator (NEMO). Therefore, TAK1 serves as a gatekeeper for a protumorigenic, NF-κB-independent function of NEMO in parenchymal liver cells.

INTRODUCTION

Inflammatory- and stress-related signaling pathways (e.g., NF-κB, c-Jun-[N]-terminal-kinase [JNK], p38[MAPK]) closely interact to modulate basic cellular processes such as hepatocyte apoptosis, proliferation, and cancer development (Wagner and Nebreda, 2009). However, the role of the NF-κB signaling pathway in the development of hepatocellular carcinoma (HCC) continues to remain controversial (Vainer et al., 2008). Inhibition of NF-κB by conditional deletion of the I-κB-kinase subunits *Ikk2*

Significance

In most instances, liver cancer arises on the basis of chronic damage and inflammation, suggesting that pharmacological modification of inflammatory signaling pathways might represent a potentially effective strategy to prevent hepatocellular carcinoma. The role of the NF-κB pathway in hepatocarcinogenesis has remained controversial. Genetic studies focusing on the NF-κB-activating IKK complex led to conflicting results when compared with studies focusing on other members of the NF-κB pathway. We demonstrate that depending on the functionality of TAK1, the IKK subunit NEMO, previously assigned as a tumor suppressor, activates a protumorigenic pathway that is independent of NF-κB. This finding reveals a functional distinction between the IKK subunits and the NF-κB pathway, which might have implications for the development of liver-cancer-preventive strategies.

(also termed *Ikkβ*) resulted in increased liver tumor formation in a chemical carcinogenesis model (Maeda et al., 2005). Moreover, conditional deletion of the regulatory IKK-subunit NF-κB essential modulator (*Nemo*) (also termed *Ikkγ*) resulted in spontaneous hepatocarcinogenesis in 12-month-old mice (Luedde et al., 2007), suggesting that NEMO functions as a tumor suppressor in the liver. Notably, a previous study targeting the superrepressor IκBα has shown that under certain conditions inhibition of the NF-κB pathway potentially inhibits the malignant transformation of hepatocytes (Pikarsky et al., 2004). In line, activation of the canonical and noncanonical NF-κB pathway by lymphotoxin promotes hepatocarcinogenesis (Haybaeck et al., 2009). Therefore, the exact role of the IKK complex and NF-κB in hepatocarcinogenesis remains controversial, and differences may be due to the mouse model and type of chronic liver damage inflicted.

The kinase transforming growth factor (TGF)-β-activated kinase 1 (TAK1) belongs to the family of mitogen-activated protein kinase kinase kinases (MAP3Ks). It is activated in response to cytokines like tumor necrosis factor (TNF), as well as by lipopolysaccharide (LPS) and TGF-β, and is involved in controlling the activation of p38MAPK, JNK, and NF-κB in various cellular systems (Rincon and Davis, 2009). Upon TNF stimulation, TAK1 and its adaptors, TAB2, TAB3, and NEMO, are recruited to polyubiquinated RIP1, thus allowing TAK1 to phosphorylate and activate the catalytic IKK subunits (Adhikari et al., 2007). Although it has been demonstrated that TAK1 is essential for innate and adaptive immune responses (Sato et al., 2005; Tang et al., 2008; Wan et al., 2006), its functional role in liver parenchymal cells remains elusive. We investigated this in the current study.

RESULTS

Spontaneous Hepatitis, Cholestasis, Hepatocyte Dysplasia, and Liver Fibrosis in Mice with Conditional Ablation of TAK1 in Liver Parenchymal Cells

To elucidate the hepatic function of TAK1 in vivo, we generated mice with conditional deletion of the *Tak1*-gene (*Map3k7*) in liver parenchymal cells (LPC) (TAK1$^{LPC\text{-}KO}$) by intercrossing TAK1 floxed mice with Alfp-Cre transgenic mice (Kellendonk et al., 2000; Sato et al., 2005). The hepatic phenotype of these animals was compared with mice with LPC-specific deletion of *Nemo* (NEMO$^{LPC\text{-}KO}$). TAK1$^{LPC\text{-}KO}$ and NEMO$^{LPC\text{-}KO}$ mice showed efficient ablation of the respective proteins in LPC, as demonstrated by western blot analysis of whole liver protein extracts (Figure 1A). By 6 weeks of age, TAK1$^{LPC\text{-}KO}$, but not NEMO$^{LPC\text{-}KO}$ mice already displayed an aberrant liver architecture with numerous small but macroscopically visible nodules (Figure 1B). This macroscopic appearance coincided with strongly elevated serum aminotransferase (ALT and AST) and bilirubin levels (mainly consisting of direct bilirubin [Figure 1C]). Additionally, elevated levels of circulating alkaline phosphatase (AP) and glutamate dehydrogenase (GLDH) were detected in 6-week-old TAK1$^{LPC\text{-}KO}$ mice (Figure 1C), indicating intrahepatic cholestasis. Compared with TAK1$^{LPC\text{-}KO}$ mice, NEMO$^{LPC\text{-}KO}$ animals displayed a milder increase in ALT/AST at this age, without significant elevation of bilirubin or cholestatic enzymes (Figure 1C).

We further examined TAK1$^{LPC\text{-}KO}$ mice at 20 weeks of age. These mice displayed an aggravated macroscopic phenotype with larger nodules and an icteric appearance (Figure 1D), correlating with elevated serum bilirubin levels as compared with age-matched wild-type (WT), NEMO$^{LPC\text{-}KO}$, as well as 6-week-old TAK1$^{LPC\text{-}KO}$ mice (Figure 1E). ALT and AST levels were still significantly upregulated in sera of 20-week-old TAK1$^{LPC\text{-}KO}$ mice, but to minor extent than at 6 weeks and to similar extent as seen in age-matched NEMO$^{LPC\text{-}KO}$ mice (Figure 1E). Finally, all TAK1$^{LPC\text{-}KO}$ mice investigated succumbed to death between 14 and 36 weeks of age (n = 9), whereas no spontaneous deaths were noticed in WT (n = 15) or NEMO$^{LPC\text{-}KO}$ mice (n = 15) within a period of 60 weeks (Figure 1F).

On histological level, numerous areas of focal hepatocyte necrosis morphologically resembling biliary infarcts could be detected in TAK1$^{LPC\text{-}KO}$, but not in WT or NEMO$^{LPC\text{-}KO}$ livers, whereas immune cell infiltrates were detected in both mutant lines, but not in WT mice (Figure 2A and Figures S1A and S1B> available online). Moreover, nodules displaying cellular features of dysplasia like anisokaryosis were detected in TAK1$^{LPC\text{-}KO}$ livers (Figure 2B). Hematoxylin and eosin and pan-cytokeratin (CK) stainings revealed the absence of biliary epithelial cells and regularly shaped small bile ducts in most portal tracts of 6- to 8-week-old TAK1$^{LPC\text{-}KO}$ compared with WT and NEMO$^{LPC\text{-}KO}$ livers (Figures 2C–2E and Figures S1A–S1C). Morphometric analyses revealed that biliary ductopenia in TAK1$^{LPC\text{-}KO}$ livers was pronounced within areas of hepatocyte dysplasia, whereas pre-existing biliary epithelial cells and bile duct structures were still—but rarely—detected in the border zone of areas with dysplasia (Figure 2E, lower panel, and Figure S1D).

Chronic hepatitis and cholestasis lead to liver fibrosis (Bataller and Brenner, 2005). At 6 weeks of age, TAK1$^{LPC\text{-}KO}$ and NEMO$^{LPC\text{-}KO}$ animals displayed signs of periportal liver fibrosis as detected by Sirius red staining, which progressed to severe diffused fibrosis in 20- to 29-week-old animals (Figures 2F and 2G). Livers of 14-week-old TAK1$^{LPC\text{-}KO}$ mice and NEMO$^{LPC\text{-}KO}$ mice showed strongly increased hydroxyproline content (Figure 2H). Moreover, livers of 6-week-old mice displayed an upregulation of collagen *Iα1* and matrix metalloprotease (*Mmp*)*-1* mRNA, further confirming the increased production of extracellular matrix (Figure S1E). TGF-β is a crucial regulator of liver fibrosis (Bataller and Brenner, 2005). All three TGF-β isoforms were strongly upregulated on mRNA-level in TAK1$^{LPC\text{-}KO}$ mice (Figure S1F). Immunohistochemistry and western blot analysis revealed that *Tgf-β* expression was leading to strong phosphorylation of SMAD2 and SMAD3 in parenchymal and nonparenchymal hepatic cells of TAK1$^{LPC\text{-}KO}$ mice (Figures S1G and S1H). Therefore, TAK1 deficiency in parenchymal liver cells results in development of hepatic fibrosis.

TAK1 Ablation in LPC Causes Spontaneous Hepatocyte Apoptosis and Hyperplasia

We further investigated how TAK1 deficiency influences hepatocyte cell death and proliferation. Despite frequent necrotic foci in livers of TAK1$^{LPC\text{-}KO}$ mice, we tested if TAK1 also influences caspase activation and spontaneous apoptosis of hepatocytes. TUNEL stains revealed dispersed and numerous TUNEL-positive cells in livers of TAK1$^{LPC\text{-}KO}$ and to a lesser extent in

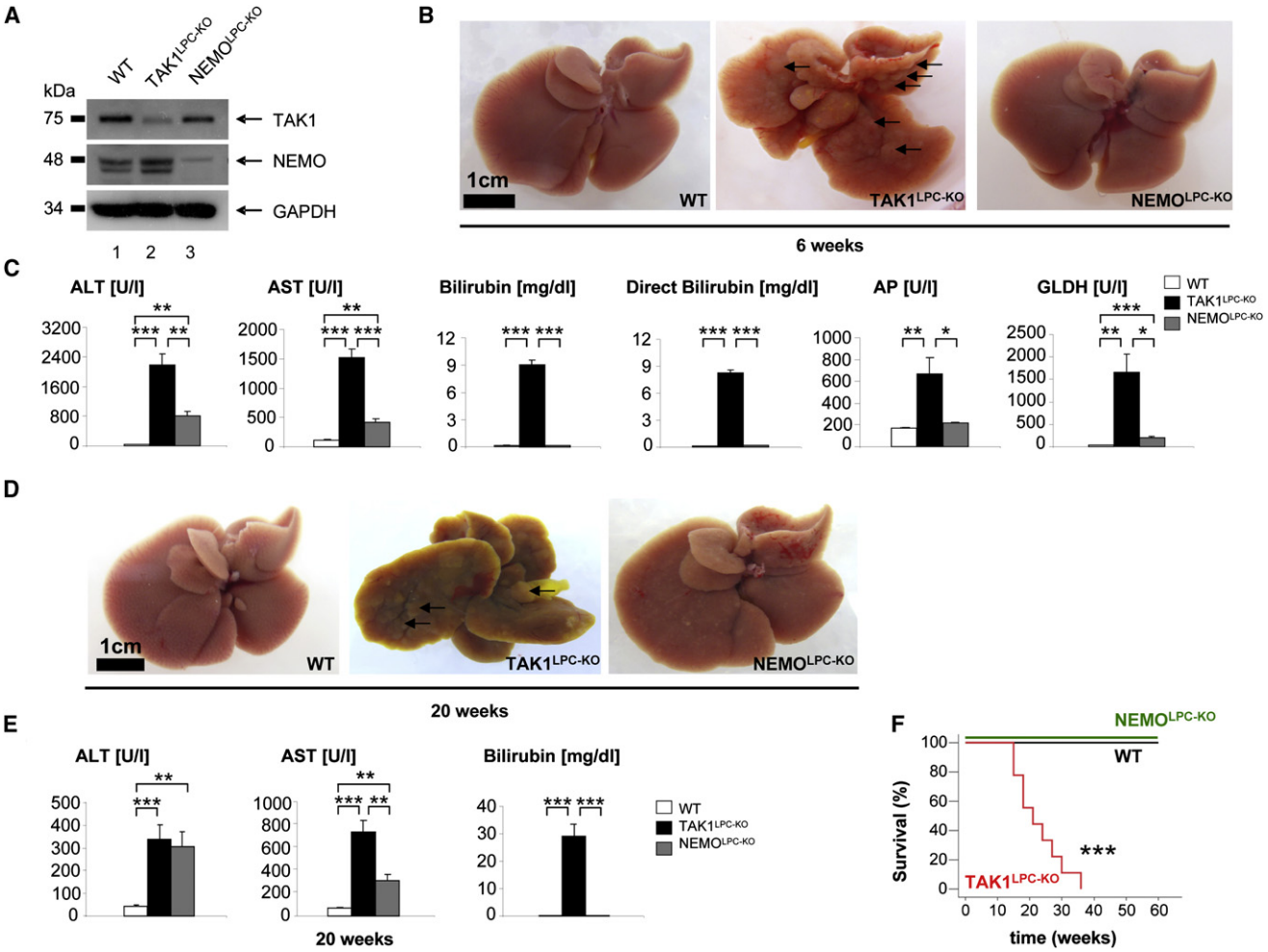

Figure 1. Spontaneous Development of Hepatocyte Damage, Cholestasis, and Spontaneous Death in TAK1^{LPC-KO} Mice

(A) Western blot analysis of whole liver protein extracts from 6-week-old male TAK1^{LPC-KO}, NEMO^{LPC-KO}, and control littermate mice (WT) using antibodies against TAK1, NEMO, and GAPDH as loading control (kDa, kilodalton).

(B) Representative macroscopic pictures of 6-week-old male WT (left panel), TAK1^{LPC-KO} (middle panel), and NEMO^{LPC-KO} livers (right panel). Small nodular structures are observed in livers of TAK1^{LPC-KO} mice (arrows).

(C) Serum level analysis of alanine aminotransferase (ALT), aspartate aminotransferase (AST), total and direct (conjugated) bilirubin, alkaline phosphatase (AP), and glutamate dehydrogenase (GLDH) in 6-week-old male mice. Results are shown as mean, error bars indicate standard error of the mean (SEM). *$p < 0.05$; **$p < 0.01$; ***$p < 0.001$ (n = 4 each genotype).

(D) Representative macroscopic pictures of a 20-week-old male WT (left panel), TAK1^{LPC-KO} (middle panel), and NEMO^{LPC-KO} mouse (right panel). Livers of TAK1^{LPC-KO} mice show multiple nodules (arrows) and a yellow, icteric color.

(E) Analysis of serum ALT, AST, and total bilirubin levels in 20-week-old male WT, TAK1^{LPC-KO}, and NEMO^{LPC-KO} mice. Results are shown as mean, error bars indicate SEM. **$p < 0.01$; ***$p < 0.001$ (n = 4 each genotype).

(F) Kaplan-Meier curve showing spontaneous death of TAK1^{LPC-KO} mice between 16 and 36 weeks of age. ***$p < 0.001$. WT n = 15, NEMO^{LPC-KO} n = 15, and TAK1^{LPC-KO} n = 9.

NEMO^{LPC-KO}, but not in WT mice. Morphologically, these cells were identified as hepatocytes (Figures 2I and 2J). Moreover, cleavage of Caspase-3, a key feature of apoptotic cell death, occurred in TAK1^{LPC-KO} and to a lesser extent in NEMO^{LPC-KO} mice but not in WT livers (Figures S1I–S1K), suggesting that TAK1 deficiency sensitizes hepatocytes to caspase-dependent apoptosis.

Hepatocyte cell death was accompanied by excessive liver cell proliferation in TAK1^{LPC-KO} mice, as demonstrated by increased BrdU incorporation (Figure 2K). Ki67 staining confirmed that this hyperproliferation could mainly be attributed to hepatocytes (Figure 2L and Figure S1L). In addition, expression of cyclin D1, cyclin E, and PCNA, key cell-cycle markers for G_1-S-phase transition, were strongly enhanced in livers of TAK1^{LPC-KO} mice (Figure S1M), underlining the correlation between hepatocyte cell death and hyperproliferation in these animals.

Early-Onset Hepatocarcinogenesis in TAK1^{LPC-KO} Mice

We further examined whether the dysplasia and hyperproliferation of hepatocytes detected in livers of TAK1^{LPC-KO} from

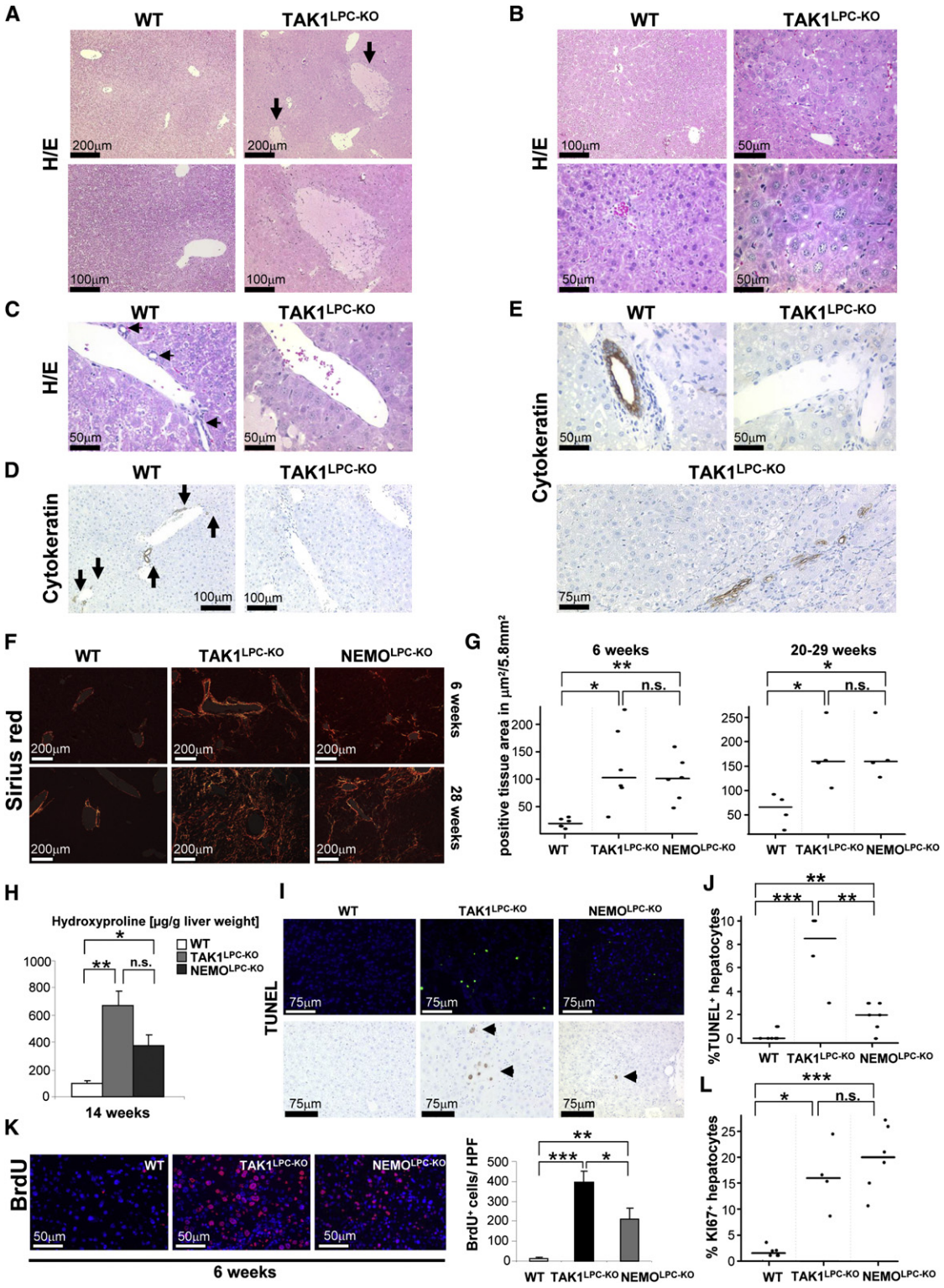

Figure 2. Focal Hepatocyte Necrosis, Reduction of Small Portal Bile Ducts, Liver Fibrosis, Increased Cell Death and Proliferation in TAK1^{LPC-KO} Mice

(A–E) Histological and immunohistochemical analysis on representative liver paraffin sections from 6-week-old male mice. (A) Multiple areas of focal hepatocyte necrosis (arrows) in livers of TAK1 mutant, but not WT animals. (B) Upper right panel: histological appearance of a nodular area with dysplasia in a TAK1^{LPC-KO} mouse, adjacent to an area with less dysplasia. Upper left panel: WT control liver. Lower panels: strong enlargement of hepatocyte-nuclei in dysplastic areas of TAK1^{LPC-KO} livers (right panel) compared with WT livers (left panel). (C and D) Hematoxylin and eosin (H&E) and Cytokeratin (CK) stainings showing the presence

6 weeks onward would lead to HCC development at later time points. Thus, we analyzed 16- to 33-week-old TAK1^{LPC-KO} mice (5 males and 11 females) for the presence of liver tumors. Notably, 14 out of 16 mice developed liver tumors, which histologically qualified as HCC (≈88% incidence) due to the following criteria: expansive and tissue infiltrating growth pattern, frequent hepatocyte mitoses, increased cellularity, nodular structures, broadening and loss of the regular collagen IV and reticulin network separating neighboring hepatocytes (Figures 3A and 3B and Table S1). Remarkably, no HCC or liver tumors were detected in 21- to 26-week-old NEMO^{LPC-KO} mice (n = 6) (Figure S2 and Table S1), which usually developed HCC at the age of around 50 weeks (Luedde et al., 2007).

We investigated microdissected TAK1^{LPC-KO} HCC (n = 19) and age-matched WT livers (n = 8) for chromosomal aberrations. Array comparative genomic hybridization analysis (aCGH) revealed chromosomal aberrations in all 19 TAK1^{LPC-KO} HCC samples (Figure 3C), indicating the neoplastic, most likely malignant nature of the tumors observed. Amplifications and deletions of chromosomal regions ranged from 0.68 megabase (MB) to 151 MB. Of note, the pattern of chromosomal aberrations showed a common signature in HCC from different individual TAK1^{LPC-KO} mice (permutation test, $p < 0.00001$). A total of 7 out of 19 HCC displayed amplifications on chromosome 4, 14 out of 19 HCC analyzed displayed amplifications on chromosome 8, and 17 out of 19 HCC displayed amplifications on chromosome 13 (often affecting the whole q-arm) (Figure 3C). This suggests a functional relationship between TAK1-dependent signals and chromosomal integrity in hepatocytes. Transcriptional analysis revealed significant upregulation of selected oncogenes and tumor-suppressor genes in microdissected HCC from TAK1^{LPC-KO} mice: among others, *FgR* and *Jun* (chromosome 4), *FgfR1* (chromosome 8), *Ntrk2* and *Net1* (chromosome 13) were upregulated when compared with WT livers (conventional t test) (Figure 3D and Table S2). However, multiple comparison with Bonferroni correction confirmed significant upregulation only for *Ntrk2* (20.58-fold), *Net1* (6.66-fold), and *Jun* (2.81-fold) (Table S2), which are all located on affected chromosomes, while many other oncogenes and tumor-suppressor genes involved in hepatocarcinogenesis (e.g., *p53*, *c-myc*, *fos*, *n-ras*) were not significantly dysregulated (Table S2).

To further understand if HCCs of TAK1^{LPC-KO} mice could be classified as malignant tumors, samples were profiled by quantitative real-time polymerase chain reaction with a 16-gene signature that identifies and stratifies liver tumors according to their degree of differentiation and proliferation rate (Cairo et al., 2008). As a control, normal liver samples, NEMO^{LPC-KO} samples as well as samples of aggressive liver tumors from WHV/N-myc2 p53^{+}/Delta mice (Renard et al., 2000) were added. Unsupervised analysis clearly showed co-clustering of nearly all the TAK1^{LPC-KO} and NEMO^{LPC-KO} nodules with control tumor samples, displaying mRNA upregulation of genes involved in proliferation and cell cycle (*Afp*, *Bub1*, *Dlg7*) and accounting for a highly transformed molecular phenotype of the samples (Figure 3E). These data further classify TAK1^{LPC-KO} liver tumors as HCC.

TAK1 Controls Hepatocyte Apoptosis and Necrosis via Distinct NF-κB-Dependent and -Independent Pathways

We further analyzed which pathways could mediate the downstream effects of TAK1 in LPC. Inducible degradation of IκBα in response to LPS-injection—a potent inducer of endogenous TNF secretion (Leist et al., 1995)—was strongly inhibited in the livers of TAK1^{LPC-KO} mice to a similar extent as observed in NEMO^{LPC-KO} mice (Figure 4A). This correlated with the inhibition of LPS-induced DNA binding of NF-κB in electrophoretic mobility shift assay analysis (Figure 4B). We furthermore isolated primary hepatocytes and stimulated them with recombinant TNF. In line with the massive hepatocyte cell death detected in vivo, primary hepatocytes isolated from TAK1^{LPC-KO} and from NEMO^{LPC-KO} mice, although to a lesser extent, showed severe morphological alterations and underwent cell death immediately upon culturing. This was not observed in cultures with hepatocytes isolated from WT mice (data not shown). Interestingly, 1 hr after TNF stimulation, TAK1- and NEMO-deficient hepatocytes demonstrated a similar defect in the induction of the NF-κB-target genes IκBα and A20 as compared with WT hepatocytes (Figure 4C). Notably, JNK was hyperactivated upon LPS-stimulation in TAK1^{LPC-KO} as compared with WT livers (Figure 4A).

of small bile ducts in portal areas of WT (arrows), but not TAK1^{LPC-KO} livers (right panels). (E) Upper panels: no CK^{+} cells can be detected in areas where a portal tract is expected in a TAK1^{LPC-KO} liver (right panel) when compared with strongly positive bile ducts in livers of WT mice (left panel). Lower panel: detection of CK^{+} cells and biliary ducts in an area surrounding a dysplastic nodule, but not within the nodule of a TAK1^{LPC-KO} liver.
(F) Representative liver sections of 6- (upper panels) and 28-week-old (lower panels) male WT, TAK1^{LPC-KO}, and NEMO^{LPC-KO} mice stained with Sirius red revealing periportal fibrosis in younger mice and severe diffuse liver fibrosis in older TAK1^{LPC-KO} mice (red: collagen deposition).
(G) Densitometric analysis of Sirius red-stained collagen strings from livers of 6- and 20- to 29-week-old WT, TAK1^{LPC-KO}, and NEMO^{LPC-KO} mice (n = 6 each genotype at 6-week-old mice, n = 4 each genotype at 20- to 29-week-old mice). Results are shown as mean, and error bars indicate standard deviation (SD); *$p < 0.05$; **$p < 0.01$.
(H) Hydroxyproline-assay quantifying the collagen content in liver. Results are shown as mean, error bars indicate SEM. *$p < 0.05$; **$p < 0.01$ (n = 3).
(I) Spontaneous hepatocyte cell death in 6-week-old TAK1^{LPC-KO} and (to lesser degree) in NEMO^{LPC-KO}, but not in WT mice, as demonstrated by TUNEL assay on liver sections (upper panels: fluorescence on frozen sections, lower panels: peroxidase staining on paraffin sections, black arrows indicate TUNEL^{+} hepatocyte nuclei).
(J) Quantification of TUNEL^{+} hepatocytes in 6-week-old mice. Results are shown as mean, and error bars indicate SEM. **$p < 0.01$; ***$p < 0.001$. (n = 7 WT; n = 4 TAK1^{LPC-KO}; n = 7 NEMO^{LPC-KO}, each dot represents the average value per mouse liver, calculated from four high-power-field [HPF] analyses).
(K) BrdU incorporation analysis to detect S phase positive liver cells of 6-week-old mice that underwent repetitive BrdU injections for 2 days (DAPI counterstaining is marked in blue). Statistical analysis of BrdU^{+} cells per HPF. Results are shown as mean, and error bars indicate SD. *$p < 0.05$; **$p < 0.01$; ***$p < 0.001$ (n = 3).
(L) Densitometric analysis of Ki67^{+} hepatocytes in the respective 6- to 9-week-old knockout mice. Results are shown as mean, and error bars indicate SEM. *$p < 0.05$; ***$p < 0.001$ (n = 6 WT; n = 4 TAK1^{LPC-KO}; n = 6 NEMO^{LPC-KO}; 10 HPF/mouse liver).
See also Figure S1.

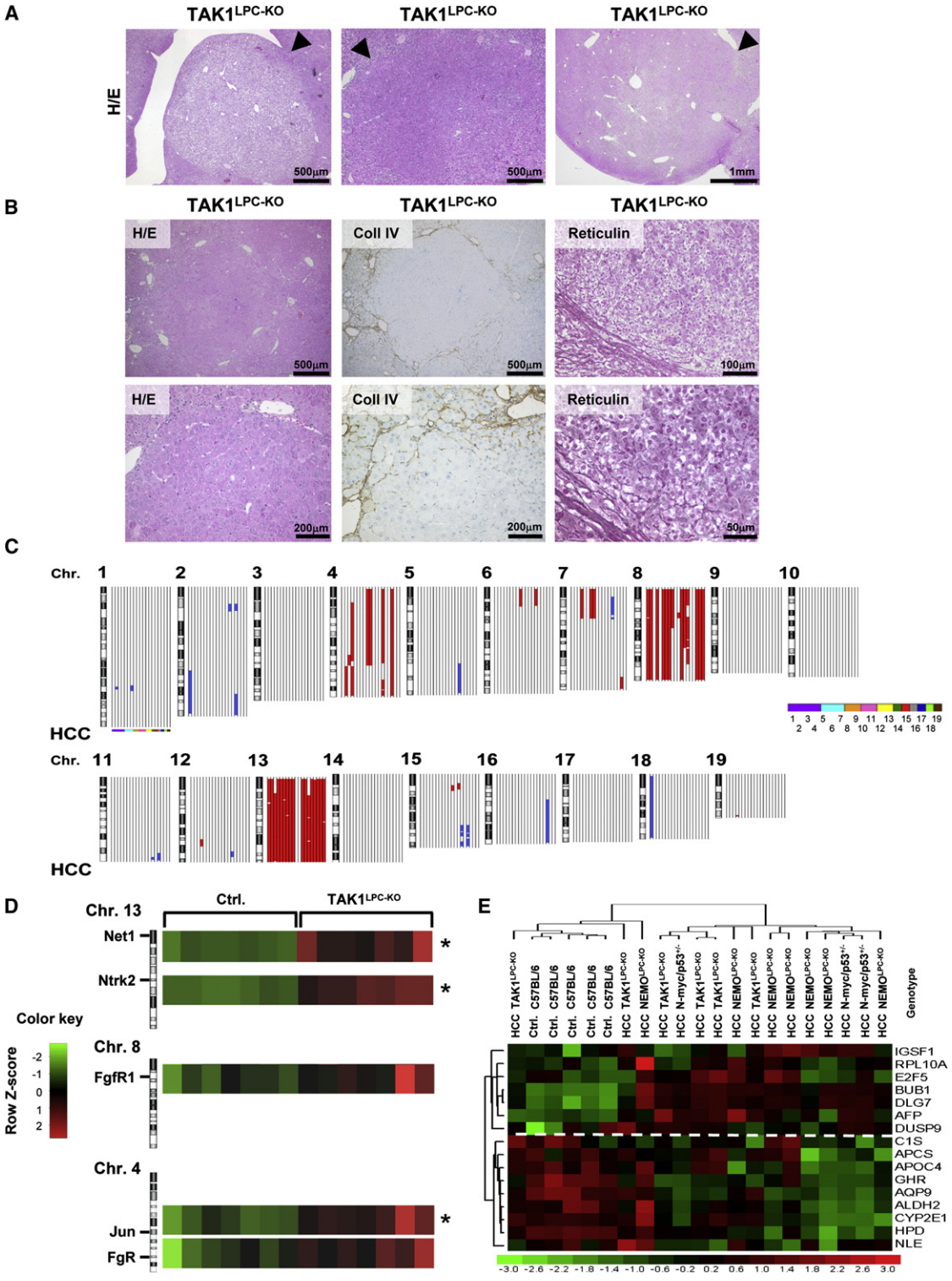

Figure 3. Early-Onset HCC Development in TAK1^{LPC-KO} Mice

(A) Histological features of different liver tumors in 16- to 33-week-old TAK1^{LPC-KO} mice stained by H/E (left panel, arrow head). Liver tumor with a "clear-cell-like" appearance. The middle and right panels show liver tumors (arrow head) of a size up to 4 mm with eosinophilic cells.

(B) Consecutive slides of a representative liver tumor in a 20-week-old TAK1^{LPC-KO} mouse stained with H/E, Collagen IV, and Silver-Reticulin, showing typical histological features of human HCC: expansive growth, increased cellularity, loss of collagen IV staining between neighboring hepatocytes and abnormal architecture, and loss of reticulin fibers.

Because it has been previously demonstrated that only complete, but not partial, inhibition of inducible NF-κB activation sensitizes hepatocytes to LPS-induced apoptosis (Luedde et al., 2007), we compared the apoptotic response following LPS stimulation in TAK1^{LPC-KO} and NEMO^{LPC-KO} mice. Correlating with inhibition of LPS-induced NF-κB activation, TAK1^{LPC-KO} mice developed massive liver cell apoptosis and liver injury 9 hr after LPS treatment similar to NEMO^{LPC-KO} mice, as demonstrated by TUNEL assay, western blot analysis for cleaved Caspase-3, and measurement of serum ALT levels (Figures 4D–4F). Therefore, TAK1 has a crucial function, similar to NEMO, in mediating LPS/TNF-induced activation of NF-κB and protection from hepatocyte apoptosis. Absence of one of both molecules—either TAK1 or NEMO—blocks NF-κB induction. However, our findings demonstrate that not only JNK can be activated in the absence of TAK1, but that TAK1 inhibits hyperactivation of JNK in response to LPS injection.

Despite spontaneous hepatocyte apoptosis, TAK1^{LPC-KO}, but not NEMO^{LPC-KO}, mice showed areas of hepatic necrosis (Figure 2A and Figure S1A). Therefore, we hypothesized that in addition to caspase-dependent apoptosis, TAK1 might withhold additional functions in controlling hepatocyte cell death, and therefore intercrossed TAK1^{LPC-KO} with floxed Caspase-8 mice (TAK1/Casp8^{LPC-KO}) (Figure S3A). Serological analysis of 6-week-old TAK1/Casp8^{LPC-KO} animals revealed a milder elevation of ALT levels and similar AST levels in these animals compared with TAK1^{LPC-KO} single mutants, whereas serum bilirubin levels were significantly higher in double mutants than in the single TAK1^{LPC-KO} mice (Figure S3B). Histologically, areas of focal necrosis were detected in TAK1/Casp8^{LPC-KO} at earlier age and even to larger extent than in TAK1^{LPC-KO} animals, probably reflecting additional proinflammatory effects of a Caspase-8 knockout in hepatocytes as previously suggested (Ben Moshe et al., 2007). These effects were accompanied by hyperproliferation, dysplasia and reduction of biliary epithelial cells within the dysplastic areas (Figure S3C). Western blot analysis confirmed a similar expression of PCNA in TAK1/Casp8^{LPC-KO} as compared with TAK1^{LPC-KO} mice (Figure S3D). However, TAK1/Casp8^{LPC-KO} mice were devoid of cleaved Caspase-3, as examined on immunohistochemical and protein level (Figures S3C and S3D). TAK1/Casp8^{LPC-KO} mice did not spontaneously die within the observed period of 32 weeks, but showed signs of growth retardation (Figure S3E). These results strongly suggest that in addition to controlling NF-κB and caspase-dependent apoptosis in hepatocytes, TAK1 also suppresses a signaling pathway that is independent of NF-κB-mediated regulation of Caspase-3 cleavage and that mediates focal necrosis, dysplasia, and biliary ductopenia in the liver.

A NEMO-Dependent but NF-κB-Independent Pathway Mediates Hepatocyte Necrosis, Dysplasia, and Biliary Alterations in TAK1^{LPC-KO} Mice

It has been proposed that complexes consisting of TAK1 and NEMO are not only involved in NF-κB activation, but might also control alternative cellular pathways (Karin and Gallagher, 2009). We therefore hypothesized that a NEMO-dependent pathway might be responsible for some of the phenotypes observed in the TAK1-deficient animals and intercrossed TAK1^{LPC-KO} with NEMO^{LPC-KO} mice to generate animals with combined deletion of TAK1 and NEMO in LPC (TAK1/NEMO^{LPC-KO}).

Surprisingly, TAK1/NEMO^{LPC-KO} mice showed macroscopically normal livers in contrast to the nodular appearance of TAK1^{LPC-KO} mice at the age of 6 weeks (Figure 5A). Moreover, the combined deletion of NEMO and TAK1 completely rescued mice from the spontaneous death observed in TAK1^{LPC-KO} mice (Figure 5B). Notably, TAK1/NEMO^{LPC-KO} mice showed the same degree of liver cell damage on a serological level as TAK1^{LPC-KO} mice, but had serum bilirubin levels similar to age-matched WT mice (Figure 5C). In correlation, electron microscopy analysis in TAK1/NEMO double mutants revealed a rescue of the severe ultrastructural signs of cholestasis that were seen in TAK1 single mutant mice (Figure S4A). Protein levels of cleaved Caspase-3 in TAK1/NEMO^{LPC-KO} mice were similar to TAK1^{LPC-KO} livers (Figure 5D). Proliferation and cell cycle markers cyclin D1 and PCNA were expressed to an analogous extent in TAK1/NEMO^{LPC-KO} and TAK1^{LPC-KO} mice, whereas cyclin E1 expression and BrdU incorporation were decreased in TAK1/NEMO^{LPC-KO} as compared with TAK1^{LPC-KO} animals (Figures 5D and Figure S4B).

Histological analysis of TAK1/NEMO^{LPC-KO} livers revealed a complete absence of necrotic and nodular dysplastic areas (Figure 5E). Moreover, TAK1/NEMO^{LPC-KO} mice maintained normal portal tract architecture and showed ubiquitous abundance of bile ducts in portal tracts (Figure 5E). Ki67 and cleaved Caspase-3^{+} cells were detected to similar extent in TAK1/NEMO^{LPC-KO} and TAK1^{LPC-KO} mice (Figures S4C–S4E). Therefore, NEMO functions to mediate focal hepatocyte necrosis, hepatocyte hyperplasia, hepatocarcinogenesis, cholestasis, and spontaneous death in TAK1^{LPC-KO} mice.

Mechanisms Driving NEMO-Dependent Dysplasia and Carcinogenesis in TAK1^{LPC-KO} Livers

To confirm that NEMO promotes hepatocyte dysplasia in 6-week-old TAK1^{LPC-KO} mice, we performed a transcriptional analysis for expression of alpha-fetoprotein (*Afp*) and *H19*, two established liver tumor markers (Ariel et al., 1998; Okuda,

(C) aCGH analysis of HCC from independent TAK1^{LPC-KO} mice. The q-arm of each chromosome is shown and chromosome numbers are indicated. Dark horizontal bars within the symbolized chromosomes represent G bands. Chromosomal deletions are indicated in blue, and amplifications in red. HCC of individual TAK1^{LPC-KO} mice were hybridized against liver tissue of an age-matched WT mouse and analyzed by aCGH analysis. Columns next to each chromosome represent individual HCC. Individual mice are labeled by horizontal colored bars (TAK1^{LPC-KO} tumors: n = 19; WT liver samples: n = 8).
(D) mRNA expression analysis of selected oncogenes located on chromosomes 4, 8, and 13. Asterisk indicates oncogenes that were significantly upregulated after multiple comparison (Bonferroni correction) (see Table S2).
(E) A 16-gene profile analysis (heat map) of HCC derived from TAK1^{LPC-KO} (20- to 31-week-old mice) and NEMO^{LPC-KO} livers (52-week-old mice). HCC were compared to aggressive liver tumors from WHV/N-myc2 p53^{+}/Delta mice. Above the dashed line the genes indicating a proliferative phenotype are listed, whereas genes below the dashed white line represent a less proliferative, more differentiated phenotype.
See also Figure S2 and Tables S1 and S2.

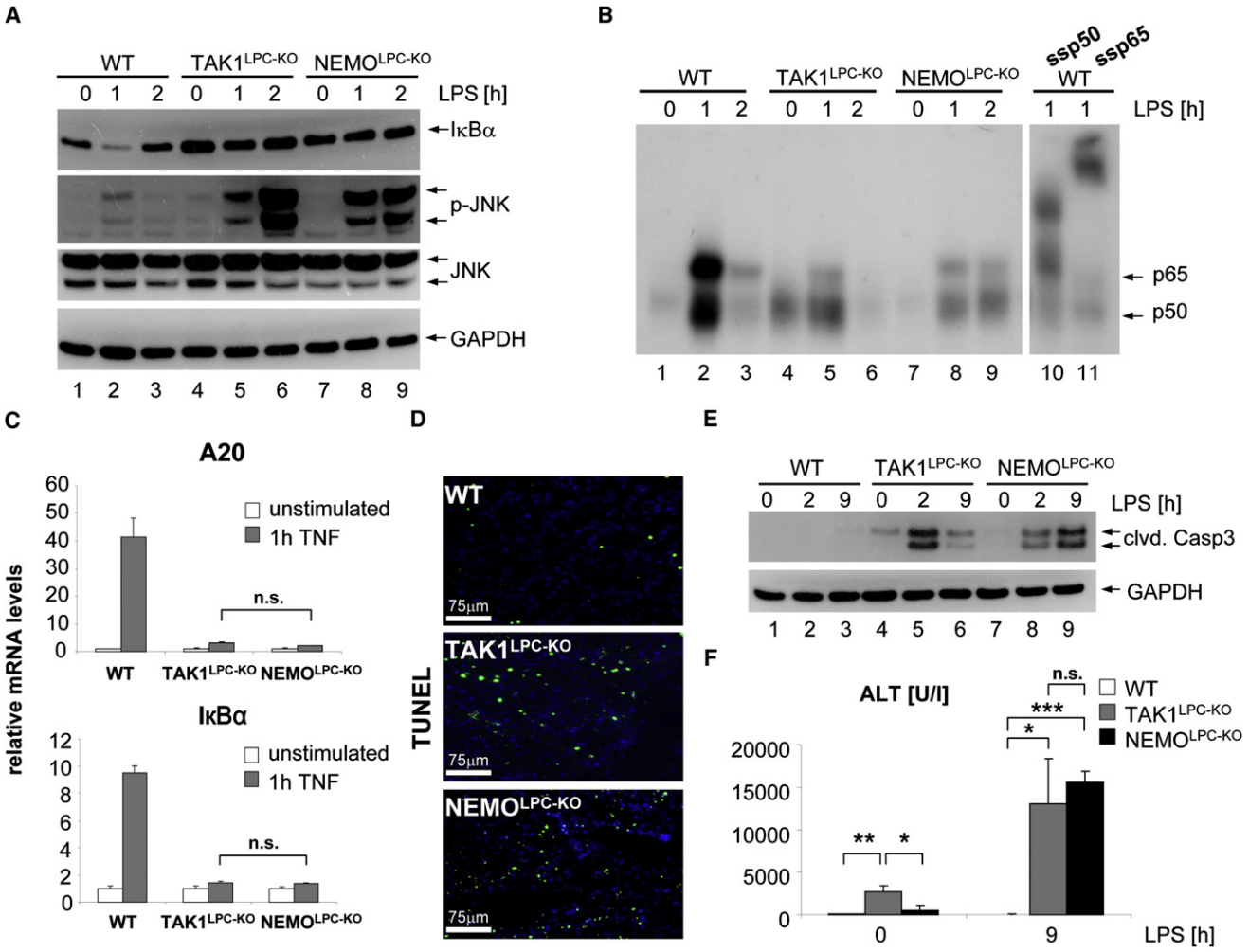

Figure 4. TAK1 Controls NF-κB- and Caspase-3-Dependent Hepatocyte Apoptosis

(A) Degradation of IκBα and phosphorylation of Jun-N-terminal-kinase (JNK) was examined by western blot analysis on liver extracts from WT, TAK1^{LPC-KO}, and NEMO^{LPC-KO} mice at the indicated time points after stimulation with bacterial lipopolysaccharides (LPS).

(B) Electrophoretic mobility shift assay (EMSA) on nuclear protein extracts from WT, TAK1^{LPC-KO} and NEMO^{LPC-KO} livers at the indicated time points after LPS stimulation. In lanes 10 and 11, antibodies against the NF-κB subunits p50 and p65 were added as supershift control. NF-κB activation in response to LPS-injection is inhibited in TAK1^{LPC-KO} and NEMO^{LPC-KO} compared with WT livers.

(C) Induction of the NF-κB target genes *A20* and *Iκbα* in response to TNF stimulation was examined in primary hepatocytes isolated from livers of WT, TAK1^{LPC-KO}, and NEMO^{LPC-KO} mice by quantitative RT-PCR. Results are expressed as mean, and error bars denote SD (n = 3 each genotype).

(D) TUNEL assay on liver sections from the indicated mouse lines at 9 hr after LPS injection (original magnification 200×).

(E) Western blot on whole liver protein extracts isolated from the indicated mouse lines after LPS-injection using an antibody against the cleaved form of Caspase-3 or GAPDH as loading control.

(F) Liver damage 9 hr after LPS-administration was assessed by measuring serum ALT. Results are expressed as mean, and error bars indicate SD. *$p < 0.05$; **$p < 0.01$; ***$p < 0.001$ (n = 3 each genotype).

See also Figure S3.

2000). TAK1^{LPC-KO} mice show dramatically increased expression of these tumor markers at 6 weeks of age when malignant tumors were not yet histologically detectable, whereas this upregulation was reversed by the additional deletion of NEMO (Figure 6A). At the age of 21 weeks, no HCC was observed in livers of TAK1/NEMO^{LPC-KO} mice (Table S1). These data demonstrate that NEMO, which has been previously assigned as a tumor suppressor in hepatocytes (Luedde et al., 2007), exhibits a previously unrecognized prodysplastic function in LPC in the absence of TAK1.

Furthermore, we set out to exclude that the rescue of the phenotype in TAK1/NEMO^{LPC-KO} animals was due to an NF-κB-dependent immune response in these animals rather than an NF-κB-independent, cell-autonomous pathway downstream of NEMO. Analysis of inflammatory cytokines revealed a strong but similar elevation of Tnf, interleukin (*Il*)-*6*, *IL-1β*, and interferon-γ (*IFNγ*) in 6-week-old TAK1 single- and TAK1/NEMO double-mutant mice compared with WT mice (Figure S5A). Moreover, flow cytometry and morphological and immunohistochemical analyses demonstrated no significant difference in the

number and quality of infiltrating immune cells between livers of TAK1^{LPC-KO} and TAK1/NEMO^{LPC-KO} mice as investigated (Figures S5B–S5E).

JNK is an important mediator of hepatocarcinogenesis (Sakurai et al., 2006), suggesting that hyperactivation of JNK in TAK1^{LPC-KO} livers in response to LPS might be an important mediator of the prodysplastic phenotype seen in these animals. Therefore, we sought to elucidate how hyperactivation of JNK is mediated in TAK1^{LPC-KO} livers. TAK1/NEMO double-mutant livers showed reduced JNK-activation in response to LPS-injection compared with TAK1 single-mutant livers (results of three independent experiments are presented in Figure 6B). Western blot analysis revealed that TAK1^{LPC-KO} livers displayed hyperactivation of the MAPK kinases MKK4 and MKK7 in response to LPS injection (Figure 6C). Thus, this mechanism in TAK1-deficient LPC is clearly distinct to hepatocytes that are solely NF-κB defective, which do not show hyperactivation of JNK by influencing MKK activity in response to TNF but rather display sustained JNK activation via inactivation of JNK-directed phosphatases (Kamata et al., 2005). Because NEMO does not withhold a known kinase activity (Hacker and Karin, 2006), we examined if TAK1 ablation might influence activity of other MAP3 kinases in hepatocytes. As shown in Figure 6C, TAK1^{LPC-KO} mice showed stronger phosphorylation of the MAP3 kinase TAO2, a known activator of MKKs and JNK upon LPS stimulation (Chen et al., 2003).

To further analyze which NEMO-dependent functions might mediate dysplasia in TAK1^{LPC-KO} animals, we tested for the phosphorylation status of known NF-κB-independent targets of the IKK complex involved in carcinogenesis (reviewed in Chariot, 2009) in the different knockout lines. No specific changes in the phosphorylation status of members of the mTOR pathway (pS6K1 and p4EBP1), of Aurora A and Dok1 were detected between TAK1^{LPC-KO} and TAK1/NEMO^{LPC-KO} mice (data not shown). However, we found increased phosphorylation of the forkhead transcription factor FOXO3a in livers of 6-week-old TAK1^{LPC-KO}, but not TAK1/NEMO^{LPC-KO} mice, which was also detected in tumors rather than in nonmalignant tissue in older TAK1^{LPC-KO} mice, but was not linked with significant changes in phosphorylation of the upstream kinase AKT (Figure 6D). Because IKK-dependent phosphorylation of FOXO3a mediates carcinogenesis in many tumors (Hu et al., 2004), this pathway might contribute to NEMO-mediated hepatocarcinogenesis in TAK1^{LPC-KO} mice.

Mechanisms Driving Cholestasis and Ductopenia in TAK1^{LPC-KO} Livers

We further analyzed the cellular mechanisms responsible for the development of cholestasis and focal ductopenia in TAK1^{LPC-KO} mice and histologically analyzed the integrity and distribution of bile ducts in livers from 4- and 8-week-old male mice. As seen in Figure 7A, 4-week-old TAK1^{LPC-KO} mice showed scattered CK$^+$ cells with morphological features of biliary epithelium and hepatic oval cells, whereas the number of these cells strongly decreased in livers of older mice (≥8 weeks of age). In contrast, TAK1/NEMO^{LPC-KO} mice displayed a strong expansion in CK$^+$ cells from 4 to 8 weeks of age, likely reflecting a sustained regenerative response of the intrahepatic biliary system to prevent ductopenia and cholestasis (Figures 7A and Figure S6A).

The Alfp-Cre line used in this study expresses Cre recombinase in LPC (hepatocytes and intrahepatic biliary epithelial cells) (Kellendonk et al., 2000), suggesting that deletion of *Tak1* in both hepatocytes and biliary epithelial cells might contribute to ductopenia in these animals. To evaluate a specific function of TAK1 in cholangiocytes, we performed co-stainings for a biliary marker (CK) together with markers of apoptosis (cleaved Caspase-3) and proliferation (Ki67) in the different knockout lines. As seen in Figure 7B, proliferation and, to a lesser extent, apoptosis were detected in cholangiocytes from TAK1^{LPC-KO} animals (Figure 7B). On ultrastructural analysis, abnormal biliary epithelial cells with light cytoplasm and partially disintegrated nuclei were detected in remnant portal bile ducts of TAK1^{LPC-KO}, but not WT or TAK1/NEMO^{LPC-KO} livers (Figure 7C), suggesting that these cells undergo cell death. We further performed laser-dissection microscopy for A6$^+$-cholangiocytes/oval cells and compared gene expression patterns between WT and TAK1^{LPC-KO} A6$^+$ cells and mice with laser-dissected WT hepatocytes. Transcriptional analysis for the expression of markers typical for oval cells and intrahepatic biliary epithelial cells (*Sca-1*, *Claudin-7*, and *Epcam*) showed strong upregulation of these markers in oval cells/cholangiocytes from WT and TAK1^{LPC-KO} mice when compared with laser-dissected WT hepatocytes, supporting the specificity of the performed laser dissection procedure (Figure 7D). Further transcriptional analysis revealed an approximately 3-fold downregulation of *Tak1* expression in cholangiocytes/oval cells from TAK1^{LPC-KO} mice when compared with WT cholangiocytes/oval cells. This confirms the expected downregulation of TAK1 in all parenchymal liver cell compartments (Figure 7D). Similar to the previous data in whole liver extracts (Figure 6A), mRNA expression of *Afp* was on average approximately 7 times higher in cholangiocytes/oval cells of TAK1^{LPC-KO} when compared with WT cholangiocytes/oval cells. In contrast, the NF-κB target gene *A20* was downregulated in average 2.4-fold in cholangiocytes/oval cells of TAK1^{LPC-KO} livers compared with WT cholangiocytes/oval cells. These results suggest that in addition to hepatocyte-specific effects, cholangiocyte-specific effects of TAK1-ablation also contribute to ductopenia in TAK1^{LPC-KO} mice and that ablation of TAK1 in cholangiocytes/oval cells influences similar signaling pathways and transcriptional targets as in hepatocytes.

We finally generated mice with parenchymal-cell specific deletion of TAK1 using an alternative solely albumin-driven Cre line (Postic and Magnuson, 2000) (TAK1Δhep) (Figure S6B). TAK1Δhep mice showed many features previously seen in TAK1^{LPC-KO} mice such as focal necrosis and hepatocyte hyperplasia and dysplasia (Figures 7E and 7F, Figures S6C and S6D). Moreover, serological analysis revealed mild hyperbilirubinemia in these animals that was not as pronounced as seen in TAK1^{LPC-KO} mice (Figure 7G) and went along with areas of ductopenia within some portal tracts (Figure 7H). It has been shown that next to hepatocytes the albumin-cre line can also lead to leaky expression of Cre-recombinase in intrahepatic cholangiocytes (Xu et al., 2006), suggesting that not only hepatocyte-specific effects of TAK1-deletion contribute to the phenotype in TAK1Δhep mice. However, some periportal areas in TAK1Δhep mice showed numerous hepatocytes that stained positive for A6, suggesting their origin from A6-positive oval cells (Figure 7H).

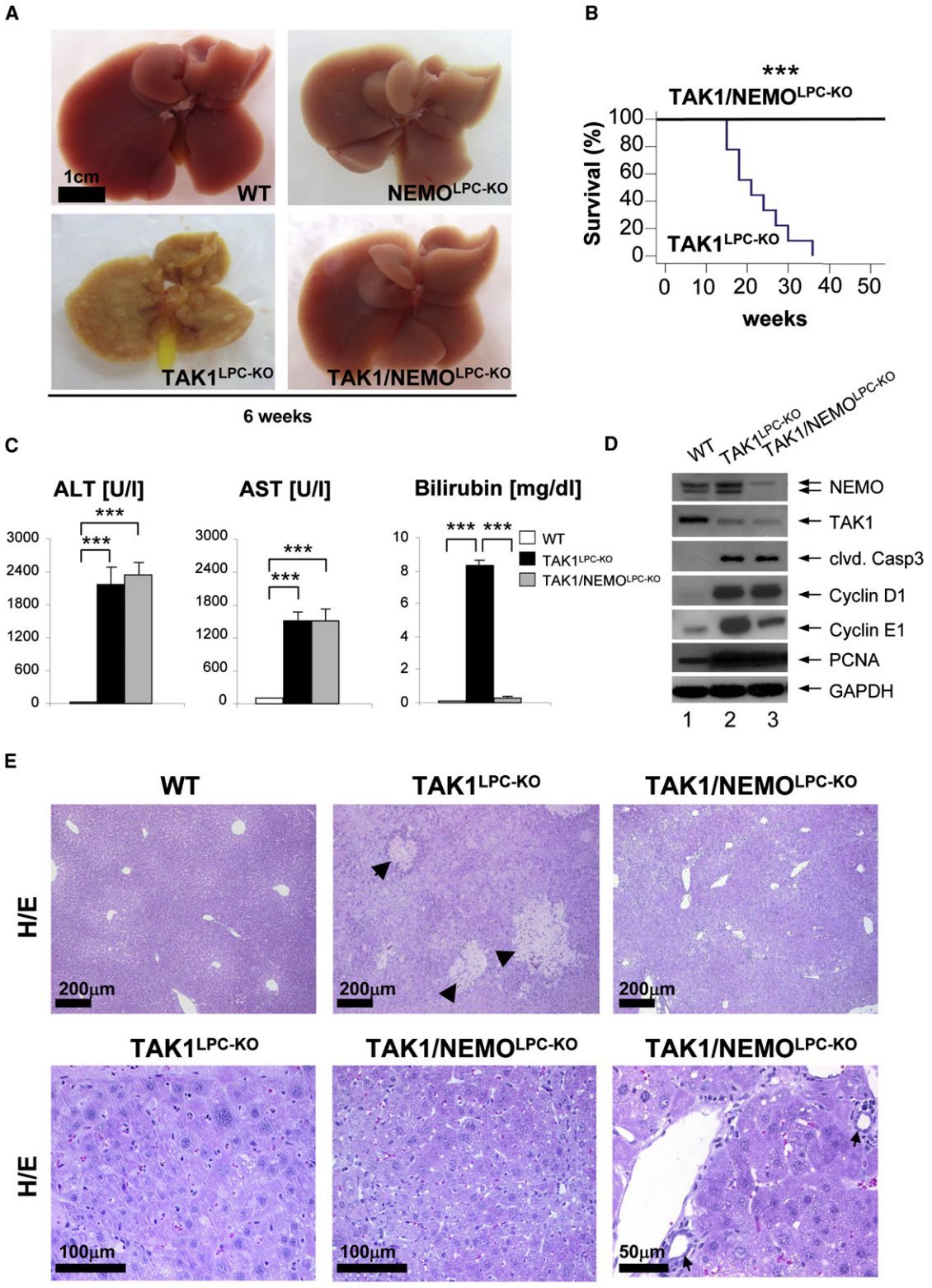

Figure 5. Additional Deletion of NEMO Prevents Cholestasis, but Not Serological Signs of Cell Death, in TAK1^{LPC-KO} Mice

(A) Representative macroscopic pictures of 6-week-old WT, TAK1^{LPC-KO}, NEMO^{LPC-KO}, and TAK1/NEMO^{LPC-KO} livers. No macroscopic alterations or small nodules could be detected in livers of double-mutant mice.

(B) Cumulative survival of TAK1^{LPC-KO} and TAK1/NEMO^{LPC-KO} mice is shown in a Kaplan-Meier curve. Additional deletion of NEMO prevents spontaneous death of TAK1^{LPC-KO} mice. ***$p < 0.001$. TAK1/NEMO^{LPC-KO} ($n = 14$) and TAK1^{LPC-KO} ($n = 9$).

Increased abundance of immature hepatocytes in TAK1Δhep animals was supported by decreased expression of epithelial markers such as *Albumin* and *C/ebp-β* (Figure S6E). These data suggest that in some areas hepatocyte dysplasia and hyperplasia might affect biliary integrity in TAK1Δhep and also TAK1^{LPC-KO} mice.

DISCUSSION

Here, we show that TAK1 controls hepatocyte apoptosis as well as necrosis and malignant transformation of hepatocytes, and that TAK1 in hepatocytes and cholangiocytes modulates biliary integrity and prevents cholestasis. Our data indicate that TAK1 is critical for the activation of NF-κB in response to TNF or LPS (Figure 8). NEMO- or TAK1-deficient hepatocytes show defective NF-κB activation in response to LPS leading to hepatocyte apoptosis and liver failure. Therefore, TAK1 and NEMO are situated in a linear pathway with nonredundant functions in NF-κB activation upon TNF or LPS stimulation. The most likely explanation for this finding is that the kinase function of TAK1 and the recruitment function of NEMO are both needed to phosphorylate the catalytic subunits IKK1 and IKK2 in response to TNF stimulation.

Mice that are not kept under axenic conditions, similar to humans, are constantly confronted with small doses of LPS originating from commensal intestinal bacteria and reaching the liver via the portal vein, where they induce cytokine production by hepatic immune cells (Enomoto et al., 2002). LPS mediates its cytotoxic effects on hepatocytes solely via TNF and its receptors (Leist et al., 1995). Because the mice described here were not kept under germ-free conditions, it is likely that TNF, which is strongly upregulated in TAK1^{LPC-KO} mice (see Figure S5A), and perhaps other TNF family members, are involved in spontaneous apoptosis and hepatitis in TAK1^{LPC-KO} and NEMO^{LPC-KO} mice. In line with this hypothesis, it was recently shown that additional deletion of TNF receptor I (TNFRI) is able to reduce liver damage and inflammation in mice with TAK1-deficient livers (Inokuchi et al., 2010).

The linear, nonredundant functions of TAK1 and NEMO in NF-κB activation explain the similar response to LPS-injection and represent one important aspect causing hepatitis in both mouse lines. However, TAK1^{LPC-KO} mice display marked differences in their phenotype as compared to NEMO^{LPC-KO} mice, such as excessive dysplasia and cancer development around 5 months earlier than NEMO^{LPC-KO} mice. Moreover, lethal cholestasis, focal hepatocyte necrosis, as well as ductopenia are found in TAK1^{LPC-KO}, but not in NEMO^{LPC-KO} mice. Therefore, TAK1 most likely controls additional pathways to hepatocarcinogenesis. Surprisingly, these additional pathways also depend on NEMO, but not on NEMO's function in NF-κB signaling: the NF-κB response (e.g., to TNF) is similarly blocked in TAK1^{LPC-KO} and NEMO^{LPC-KO}, but the additional deletion of *Nemo* rescues TAK1^{LPC-KO} mice from dysplasia, necrosis, ductopenia, cholestasis and early onset of liver carcinogenesis. These data demonstrate on a genetic level that TAK1 acts as a gatekeeper for distinct NEMO functions in hepatocarcinogenesis. In hepatocytes with functional TAK1, NEMO acts as a tumor suppressor by activating NF-κB and preventing spontaneous Caspase-8- and −3-dependent hepatocyte apoptosis and compensatory regeneration, reflected by hepatocarcinogenesis in 12-month-old NEMO^{LPC-KO} mice (Luedde et al., 2007). In contrast, the absence of TAK1 switches the function of NEMO in hepatocarcinogenesis toward a tumor-promoting role, because it mediates massive hepatocyte dysplasia and early carcinogenesis in an NF-κB-independent manner (Figure 8).

NEMO as well as TAK1 are recruited to the TNF receptor and TRAFs via the adaptor protein RIP1 (Adhikari et al., 2007), whereas receptors that do not rely on RIP1 can recruit TAK1 and NEMO directly via TRAF6 (Karin and Gallagher, 2009). We provide evidence that absence of TAK1 may promote increased NEMO-dependent recruitment and activation of other MAP3 kinases to RIP1 and/or TRAF proteins, which might lead to a functional gain of these NEMO/RIP1- or NEMO/TRAF complexes in hepatocarcinogenesis. In line with this hypothesis, TAK1^{LPC-KO} mice demonstrated a strong increase in MKK4/7 and JNK activation in their livers in response to LPS-injection, which might contribute to dysplasia and carcinogenesis (Sakurai et al., 2006). Although increased JNK activation in TAK1-defective livers correlated with increased phosphorylation of the MAP3 kinase TAO2, it is likely that also other MAP3 kinases (like MEKK1, MEKK3, and other candidates) are hyperphosphorylated in these cells and might contribute to increased JNK phosphorylation. Moreover, the functional gain of NEMO in the absence of TAK1 might also be associated with recruitment of additional RIP1 proteins to the RIP1/NEMO complex influencing necrotic cell death as recently suggested (Cho et al., 2009). We finally provided evidence for a possible role of IKK-dependent phosphorylation of FOXO3a in hepatocarcinogenesis in TAK1^{LPC-KO} mice. It is presently unclear how increased FOXO3a phosphorylation is mediated in TAK1-deficient livers, but our data in TAK1/NEMO^{LPC-KO} mice suggest that this process occurs in an IKK-dependent manner. In previous studies, direct interactions with other FOXO proteins have been proposed for TAK1 via Nemo-like kinase (Kim et al., 2010) as well as for JNK (Essers et al., 2004). The exact molecular interactions between TAK1 and FOXO3a and the functional role of FOXO3a in the TAK1^{LPC-KO} tumor model need to be clarified in future genetic studies.

(C) Analysis of serum ALT, AST, and bilirubin levels in 6-week-old TAK1^{LPC-KO} and TAK1/NEMO^{LPC-KO} mice. Results are shown as mean, and error bars denote SEM (n = 4 each genotype). ***$p < 0.001$.

(D) Western blot analysis of whole liver protein extracts from TAK1^{LPC-KO}, TAK1/NEMO^{LPC-KO}, and littermate control mice (WT), using the indicated antibodies. GAPDH served as loading control.

(E) Histological analysis of livers derived from male WT, TAK1^{LPC-KO}, and TAK1/NEMO^{LPC-KO} mice at 6 weeks of age. Upper row: areas of focal hepatocyte necrosis are seen in TAK1^{LPC-KO} mice (arrowheads), whereas TAK1/NEMO^{LPC-KO} mice show a complete absence of necrosis. Lower row: TAK1/NEMO^{LPC-KO} mice did not show areas of nodular hyperplasia with enlarged nuclei as seen in TAK1^{LPC-KO} mice. In portal tracts, biliary structures can be identified in TAK1/NEMO^{LPC-KO} mice (arrows).

See also Figure S4.

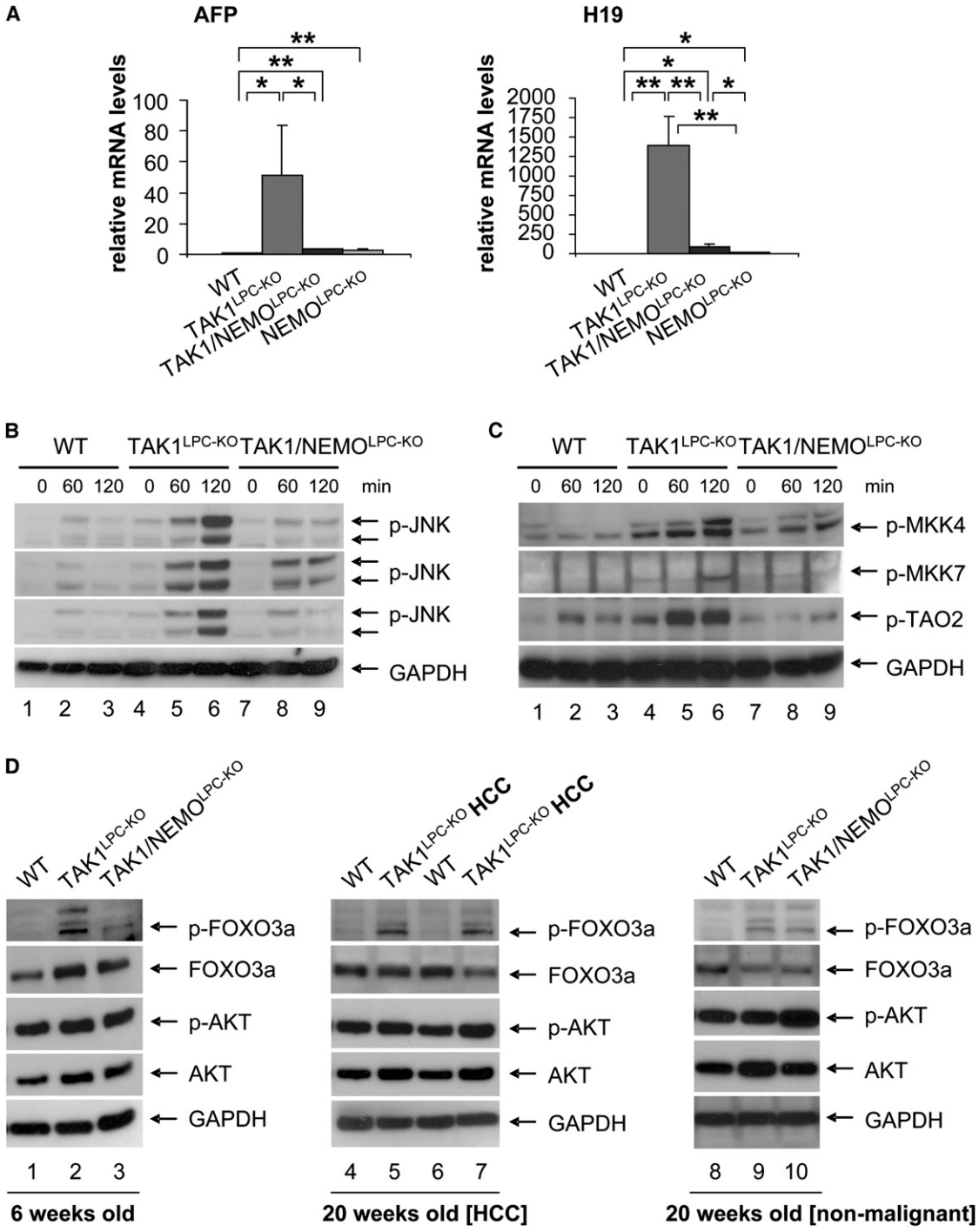

Figure 6. Mechanisms Driving NEMO-Dependent Dysplasia and Carcinogenesis in TAK1^{LPC-KO} Livers

(A) Quantitative real-time polymerase chain reaction (RT-PCR) analysis on the expression of *alpha-fetoprotein* (*Afp*) and *H19*. All values were normalized to β-actin expression. Results are expressed as mean, and error bars denote SEM. *$p < 0.05$; **$p < 0.01$ ($n = 5$ each genotype).

(B) JNK phosphorylation was assessed by immunoblot analysis of liver protein extracts from TAK1^{LPC-KO}, TAK1/NEMO^{LPC-KO}, and their respective littermate control mice at the indicated time points after LPS administration using antibodies against phosphorylated JNK, using GAPDH as loading control.

(C) Immunoblot analysis on whole liver protein extracts isolated from the indicated mouse lines after LPS-injection using antibodies detecting the phosphorylated forms of MKK4, MKK7 and TAO2 using GAPDH as loading control.

(D) Immunoblot analysis of p-FOXO3a, total FOXO3a, p-AKT, and total AKT in liver homogenates of 6-week-old TAK1^{LPC-KO}, TAK1/NEMO^{LPC-KO}, and their respective littermate control mice (left panel), extracts from dissected liver tumors, and age-matched WT-tissue (middle panel), as well as nonmalignant age-matched liver tissue (right panel). GAPDH was used as loading control.

See also Figure S5.

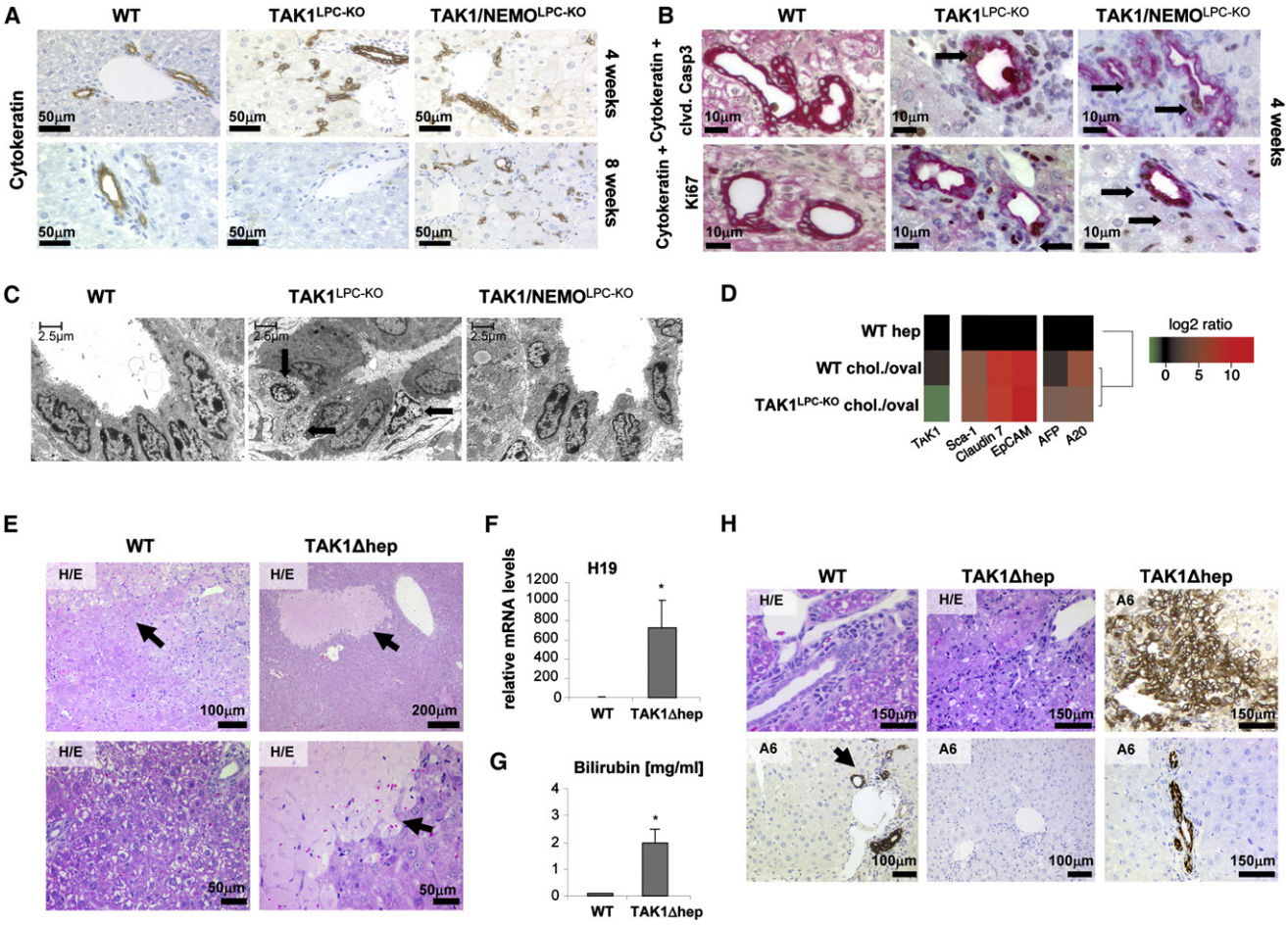

Figure 7. Mechanisms Driving Cholestasis and Ductopenia in TAK1^{LPC-KO} Livers

(A and B) Histological and immunohistochemical analysis on representative liver paraffin sections from 4- to 8-week-old male mice. (A) Upper panels: immunohistochemistry for CK demonstrates the presence of small bile ducts in portal areas of 4-week-old WT, TAK1^{LPC-KO}, and TAK1/NEMO^{LPC-KO} livers. Lower panels: TAK1^{LPC-KO} mice, but not TAK1/NEMO^{LPC-KO}, mice displayed a clear reduction of small bile ducts at the age of 8 weeks (B) Double stainings of CK with cleaved Caspase-3 or Ki67 revealed an enhanced proliferation along with apoptosis in the area of portal bile ducts of TAK1^{LPC-KO} and TAK1/NEMO^{LPC-KO} livers (arrows indicate the area of double-stained cells).

(C) Representative EM analysis of bile duct epithelial cells in livers of WT, TAK1^{LPC-KO}, and TAK1/NEMO^{LPC-KO} mice. The arrows designate epithelial bile duct cells undergoing cell death.

(D) Real-time PCR analysis on RNA from laser-dissected A6^{+} oval cells/cholangiocytes derived from WT and TAK1^{LPC-KO} livers, as well as WT hepatocytes. Expression of *Tak1*, *Sca-1*, *Claudin 7*, *Epcam*, *Afp*, and *A20* in cholangiocytes/oval cells and hepatocytes is presented as a heat map.

(E) Representative H/E staining of livers from WT and TAK1Δhep mice. The TAK1Δhep mice showed distinct necrotic areas (arrows).

(F) Quantitative RT-PCR analysis on the expression of *H19*. All values were normalized to β-actin expression. Results are expressed as mean, and error bars denote SEM. *$p < 0.05$; ($n = 5$ each genotype).

(G) Serum level analysis of total bilirubin in 9-week-old TAK1Δhep and WT mice. Results are shown as mean, and error bars indicate SEM. *$p < 0.05$ ($n = 4$ each genotype).

(H) Histological and immunohistochemical analysis of representative liver sections from 9-week-old TAK1Δhep mice and WT controls. On A6 staining, biliary ducts were absent in some portal tracts but could be detected in others (lower row). In some areas, hepatocytes stained strongly positive for A6 (upper right picture).

See also Figure S6.

Genetic characterization of liver tumors in TAK1^{LPC-KO} mice revealed an intriguing chromosomal signature, because > 85% of all investigated HCC displayed amplifications of the whole chromosome 13 or large portions of it. Moreover, large amplifications of chromosomes 4 and 8 were also detected in a smaller proportion of TAK1^{LPC-KO} livers. Interestingly, a specific signature was not seen in liver tumors from NEMO^{LPC-KO} mice (data not shown). A further in-detail characterization of the proliferation and differentiation of TAK1^{LPC-KO} HCC clearly indicated a high proliferation status of TAK1^{LPC-KO} HCC, whereas NEMO $^{LPC-KO}$ HCC were less proliferative but more differentiated. It has been previously suggested that IKK subunits might play a role for the maintenance of genome integrity in an NF-κB-independent manner (Irelan et al., 2007). Thus, further studies might reveal a specific molecular connection between the TAK1/NEMO complex and the chromosomal replication machinery, underlining

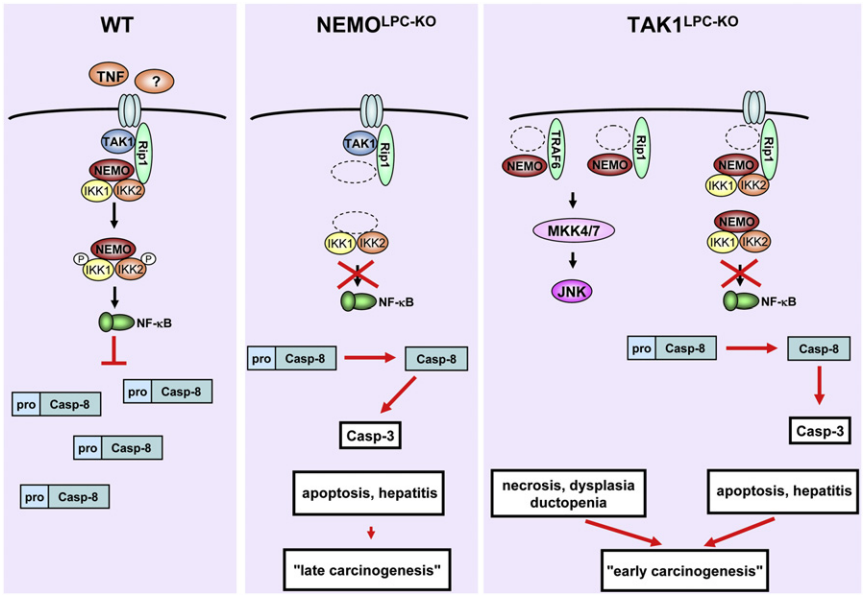

Figure 8. TAK1 Suppresses a Procarcinogenic Function of NEMO in Hepatocarcinogenesis

A simplified model for the roles of TAK1 and NEMO in hepatocarcinogenesis. Left panel: in WT hepatocytes, TAK1 and NEMO act in a linear signaling pathway to activate NF-κB. The catalytic IKK subunits are recruited to the receptor and RIP1 via NEMO. Activated NF-κB inhibits cleavage of pro-Caspase-8. In mice with defective NEMO, IKK1 and IKK2 cannot be recruited to the receptor and TAK1, leading to blockage of NF-κB activation and subsequently cleavage of pro-Caspase-8 to active Caspase-8. Further cleavage of Caspase-3 results in hepatocyte apoptosis associated with hepatitis and finally hepatocarcinogenesis in 12-month-old NEMO^{LPC-KO} mice (assigned as "late carcinogenesis"). Right panel: in TAK1-defective hepatocytes, the IKK complex is not activated in response to stimulation, which is likely caused by the absence of the TAK1-dependent kinase activity. Like in NEMO-defective hepatocytes (middle panel), the NF-κB pathway cannot be activated. However, absence of TAK1 results in a functional gain of NEMO and hyperactivation of JNK via MKK4 and MKK7. The functional gain of NEMO is associated with necrosis, dysplasia of hepatocytes, biliary ductopenia, and early HCC development already in 6- to 7-month-old TAK1^{LPC-KO} livers.

the future potential of the TAK1^{LPC-KO} liver cancer model for evaluating the molecular connection between inflammation and cancer development.

Our results shed light on the controversial debate on the function of the NF-κB pathway in hepatocarcinogenesis. It has been demonstrated that inhibition of NF-κB by conditional expression of the IκBα superrepressor in hepatocytes inhibited the development of liver cancer, suggesting a procarcinogenic function of NF-κB (Pikarsky et al., 2004). However, later studies targeting the IKK subunits IKK2 and NEMO had implied a tumor-suppressor function of this pathway in hepatocarcinogenesis (Luedde et al., 2007; Maeda et al., 2005). The reason for these apparently conflicting results has not been clarified to date. Our results demonstrate that IKK subunits can have distinct and partly opposing functions from the NF-κB pathway in hepatocarcinogenesis, because NEMO acts as a tumor promoter in TAK1-deficient hepatocytes independently of NF-κB. Consequently, TAK1 might also receive a gain of function in NEMO^{LPC-KO} mice and may potentially mediate procarcinogenic effects that are absent in the presence of NEMO. Further elucidation of NEMO-dependent functions in hepatocarcinogenesis promises to reveal specific candidates for prevention and treatment of liver cancer.

EXPERIMENTAL PROCEDURES

Generation of Conditional Knockout Mice for TAK1, NEMO, TAK1/NEMO, and TAK1/Caspase-8

Mice carrying loxP-site-flanked (floxed) alleles of the TAK1 gene *Map3k7* (*Tak1*^{Fl}) (Sato et al., 2005) and the *Nemo* gene (*Nemo*^{Fl}) (Beraza et al., 2009) were crossed to *Alfp*-Cre transgenic mice (Kellendonk et al., 2000) to generate a liver parenchymal cell-specific knockout of the respective genes (TAK1^{LPC-KO}, NEMO^{LPC-KO}). Mice carrying floxed Caspase-8-allels (Casp8^{Fl}) were generated (C.L., unpublished data). Mice with double-knockout of *Map3k7/Nemo* (TAK1/NEMO^{LPC-KO}) and *Map3k7/Caspase-8* (TAK1/Casp8^{LPC-KO}) in LPC were generated by intercrossing the respective lines. For generation of TAK1Δhep mice, *Tak1*^{Fl} mice were crossed to *Alb*-Cre transgenic mice (Postic and Magnuson, 2000). In all experiments, littermates carrying the respective loxP-flanked alleles but lacking expression of Cre recombinase were used as WT controls. Mice were bred on a mixed C57/BL6-SV129Ola genetic background. Only sex-matched animals were compared. All animal experiments were approved by the Federal Ministry for Nature, Environment and Consumers' Protection of the state of North Rhine-Westphalia and were performed in accordance to the respective national, federal, and institutional regulations.

Liver Injury Models

Liver injury experiments were performed on mice between 6 and 8 weeks of age. LPS (Sigma) was administered intraperitoneally at a concentration of 25 μg/10 g body weight. Serum ALT, AST, AP, and GLDH activities as well as total and direct serum bilirubin levels were measured by standard procedures in the Institute of Clinical Chemistry of the RWTH University Hospital Aachen. Primary hepatocytes were isolated and cultured as previously described (Luedde et al., 2008) and stimulated with murine recombinant TNF (10 ng/ml).

Statistics

Results are expressed as the mean and standard error of the mean or standard deviation as indicated. Statistical significance between experimental groups was assessed using an unpaired two-sample t test (Excel). For analysis of oncogenes and tumor-suppressor genes in HCC from TAK1^{LPC-KO} mice, we performed: (1) unpaired t test, (2) unpaired t test with log transformation of the calculated fold change values, and (3) multiple comparison analysis, for which p values underwent Bonferroni correction. For survival analyses, Kaplan-Meier survival curves were generated using SPSS software, and statistical significance was assessed by performing a Cox regression analysis (SPSS). Statistical calculation of bile ducts was assessed by using a Wilcoxon rank test.

ACCESSION NUMBERS

The aCGH data have been deposited to the Gene Expression Omnibus database under accession number GSE19105.

SUPPLEMENTAL INFORMATION

Supplemental Information includes six figures, two tables, and Supplemental Experimental Procedures and can be found with this article online at doi:10.1016/j.ccr.2010.03.021.

ACKNOWLEDGMENTS

We thank K. Kreggenwinkel, S. Behnke, B. Riepl, and Prof. Seifert for excellent technical assistance. This work was supported by grants from the European Research Council within the FP-7 (ERC-2007-Stg/208237-Luedde-Med3-Aachen, to T.L.), the German-Research-Foundation (SFB/TRR57, Project P06; P09; Ta434/2-1, to T.L. and F.T.), the Ernst-Jung-Foundation/Hamburg (to T.L.), the Interdisciplinary-Centre-for-Clinical-Research "BIOMAT" at the RWTH/Aachen (to T.L.), the Oncosuisse Foundation (OCS 02113-08-2007 to M.H.), the Julius-Müller Foundation (to M.H.), the Novartis Foundation for Biomedical Research (EMDO to M.H. and Y.B.), and the Prof. Dr. Max Cloëtta Foundation (to M.H.).

Received: September 15, 2009
Revised: December 17, 2009
Accepted: April 12, 2010
Published: May 17, 2010

REFERENCES

Adhikari, A., Xu, M., and Chen, Z.J. (2007). Ubiquitin-mediated activation of TAK1 and IKK. Oncogene *26*, 3214–3226.

Ariel, I., Miao, H.Q., Ji, X.R., Schneider, T., Roll, D., de Groot, N., Hochberg, A., and Ayesh, S. (1998). Imprinted H19 oncofetal RNA is a candidate tumour marker for hepatocellular carcinoma. Mol. Pathol. *51*, 21–25.

Bataller, R., and Brenner, D.A. (2005). Liver fibrosis. J. Clin. Invest. *115*, 209–218.

Ben Moshe, T., Barash, H., Kang, T.B., Kim, J.C., Kovalenko, A., Gross, E., Schuchmann, M., Abramovitch, R., Galun, E., and Wallach, D. (2007). Role of caspase-8 in hepatocyte response to infection and injury in mice. Hepatology *45*, 1014–1024.

Beraza, N., Malato, Y., Sander, L.E., Al-Masaoudi, M., Freimuth, J., Riethmacher, D., Gores, G.J., Roskams, T., Liedtke, C., and Trautwein, C. (2009). Hepatocyte-specific NEMO deletion promotes NK/NKT cell- and TRAIL-dependent liver damage. J. Exp. Med. *206*, 1727–1737.

Cairo, S., Armengol, C., De Reynies, A., Wei, Y., Thomas, E., Renard, C.A., Goga, A., Balakrishnan, A., Semeraro, M., Gresh, L., et al. (2008). Hepatic stem-like phenotype and interplay of Wnt/beta-catenin and Myc signaling in aggressive childhood liver cancer. Cancer Cell *14*, 471–484.

Chariot, A. (2009). The NF-kappaB-independent functions of IKK subunits in immunity and cancer. Trends Cell Biol. *19*, 404–413.

Chen, Z., Raman, M., Chen, L., Lee, S.F., Gilman, A.G., and Cobb, M.H. (2003). TAO (thousand-and-one amino acid) protein kinases mediate signaling from carbachol to p38 mitogen-activated protein kinase and ternary complex factors. J. Biol. Chem. *278*, 22278–22283.

Cho, Y.S., Challa, S., Moquin, D., Genga, R., Ray, T.D., Guildford, M., and Chan, F.K. (2009). Phosphorylation-driven assembly of the RIP1-RIP3 complex regulates programmed necrosis and virus-induced inflammation. Cell *137*, 1112–1123.

Enomoto, N., Takei, Y., Hirose, M., Ikejima, K., Miwa, H., Kitamura, T., and Sato, N. (2002). Thalidomide prevents alcoholic liver injury in rats through suppression of Kupffer cell sensitization and TNF-alpha production. Gastroenterology *123*, 291–300.

Essers, M.A., Weijzen, S., de Vries-Smits, A.M., Saarloos, I., de Ruiter, N.D., Bos, J.L., and Burgering, B.M. (2004). FOXO transcription factor activation by oxidative stress mediated by the small GTPase Ral and JNK. EMBO J. *23*, 4802–4812.

Hacker, H., and Karin, M. (2006). Regulation and function of IKK and IKK-related kinases. Sci. STKE *2006*, re13.

Haybaeck, J., Zeller, N., Wolf, M.J., Weber, A., Wagner, U., Kurrer, M.O., Bremer, J., Iezzi, G., Graf, R., Clavien, P.A., et al. (2009). A lymphotoxin-driven pathway to hepatocellular carcinoma. Cancer Cell *16*, 295–308.

Hu, M.C., Lee, D.F., Xia, W., Golfman, L.S., Ou-Yang, F., Yang, J.Y., Zou, Y., Bao, S., Hanada, N., Saso, H., et al. (2004). IkappaB kinase promotes tumorigenesis through inhibition of forkhead FOXO3a. Cell *117*, 225–237.

Inokuchi, S., Aoyama, T., Miura, K., Osterreicher, C.H., Kodama, Y., Miyai, K., Akira, S., Brenner, D.A., and Seki, E. (2010). Disruption of TAK1 in hepatocytes causes hepatic injury, inflammation, fibrosis, and carcinogenesis. Proc. Natl. Acad. Sci. USA *107*, 844–849.

Irelan, J.T., Murphy, T.J., DeJesus, P.D., Teo, H., Xu, D., Gomez-Ferreria, M.A., Zhou, Y., Miraglia, L.J., Rines, D.R., Verma, I.M., et al. (2007). A role for IkappaB kinase 2 in bipolar spindle assembly. Proc. Natl. Acad. Sci. USA *104*, 16940–16945.

Kamata, H., Honda, S., Maeda, S., Chang, L., Hirata, H., and Karin, M. (2005). Reactive oxygen species promote TNFalpha-induced death and sustained JNK activation by inhibiting MAP kinase phosphatases. Cell *120*, 649–661.

Karin, M., and Gallagher, E. (2009). TNFR signaling: ubiquitin-conjugated TRAFfic signals control stop-and-go for MAPK signaling complexes. Immunol. Rev. *228*, 225–240.

Kellendonk, C., Opherk, C., Anlag, K., Schutz, G., and Tronche, F. (2000). Hepatocyte-specific expression of Cre recombinase. Genesis *26*, 151–153.

Kim, S., Kim, Y., Lee, J., and Chung, J. (2010). Regulation of FOXO1 by TAK1-NLK pathway. J. Biol. Chem. *285*, 8122–8129.

Leist, M., Gantner, F., Bohlinger, I., Tiegs, G., Germann, P.G., and Wendel, A. (1995). Tumor necrosis factor-induced hepatocyte apoptosis precedes liver failure in experimental murine shock models. Am. J. Pathol. *146*, 1220–1234.

Luedde, T., Beraza, N., Kotsikoris, V., van Loo, G., Nenci, A., De Vos, R., Roskams, T., Trautwein, C., and Pasparakis, M. (2007). Deletion of NEMO/IKK-gamma in Liver Parenchymal Cells Causes Steatohepatitis and Hepatocellular Carcinoma. Cancer Cell *11*, 119–132.

Luedde, T., Heinrichsdorff, J., De Lorenzi, R., De Vos, R., Roskams, T., and Pasparakis, M. (2008). IKK1 and IKK2 cooperate to maintain bile duct integrity in the liver. Proc. Natl. Acad. Sci. USA *105*, 9733–9738.

Maeda, S., Kamata, H., Luo, J.L., Leffert, H., and Karin, M. (2005). IKKbeta couples hepatocyte death to cytokine-driven compensatory proliferation that promotes chemical hepatocarcinogenesis. Cell *121*, 977–990.

Okuda, K. (2000). Hepatocellular carcinoma. J. Hepatol. *32*, 225–237.

Pikarsky, E., Porat, R.M., Stein, I., Abramovitch, R., Amit, S., Kasem, S., Gutkovich-Pyest, E., Urieli-Shoval, S., Galun, E., and Ben Neriah, Y. (2004). NF-kappaB functions as a tumour promoter in inflammation-associated cancer. Nature *431*, 461–466.

Postic, C., and Magnuson, M.A. (2000). DNA excision in liver by an albumin-Cre transgene occurs progressively with age. Genesis *26*, 149–150.

Renard, C.A., Fourel, G., Bralet, M.P., Degott, C., De La Coste, A., Perret, C., Tiollais, P., and Buendia, M.A. (2000). Hepatocellular carcinoma in WHV/N-myc2 transgenic mice: oncogenic mutations of beta-catenin and synergistic effect of p53 null alleles. Oncogene *19*, 2678–2686.

Rincon, M., and Davis, R.J. (2009). Regulation of the immune response by stress-activated protein kinases. Immunol. Rev. *228*, 212–224.

Sakurai, T., Maeda, S., Chang, L., and Karin, M. (2006). Loss of hepatic NF-kappa B activity enhances chemical hepatocarcinogenesis through sustained c-Jun N-terminal kinase 1 activation. Proc. Natl. Acad. Sci. USA *103*, 10544–10551.

Sato, S., Sanjo, H., Takeda, K., Ninomiya-Tsuji, J., Yamamoto, M., Kawai, T., Matsumoto, K., Takeuchi, O., and Akira, S. (2005). Essential function for the kinase TAK1 in innate and adaptive immune responses. Nat. Immunol. *6*, 1087–1095.

Tang, M., Wei, X., Guo, Y., Breslin, P., Zhang, S., Wei, W., Xia, Z., Diaz, M., Akira, S., and Zhang, J. (2008). TAK1 is required for the survival of hematopoietic cells and hepatocytes in mice. J. Exp. Med. *205*, 1611–1619.

Vainer, G.W., Pikarsky, E., and Ben-Neriah, Y. (2008). Contradictory functions of NF-kappaB in liver physiology and cancer. Cancer Lett. *267*, 182–188.

Wagner, E.F., and Nebreda, A.R. (2009). Signal integration by JNK and p38 MAPK pathways in cancer development. Nat. Rev. Cancer *9*, 537–549.

Wan, Y.Y., Chi, H., Xie, M., Schneider, M.D., and Flavell, R.A. (2006). The kinase TAK1 integrates antigen and cytokine receptor signaling for T cell development, survival and function. Nat. Immunol. *7*, 851–858.

Xu, X., Kobayashi, S., Qiao, W., Li, C., Xiao, C., Radaeva, S., Stiles, B., Wang, R.H., Ohara, N., Yoshino, T., et al. (2006). Induction of intrahepatic cholangiocellular carcinoma by liver-specific disruption of Smad4 and Pten in mice. J. Clin. Invest. *116*, 1843–1852.